NASA

NASA-OAI

OAI
Leveraging Resources Through Collaboration

Collaborative Aerospace Research and Fellowship Program

at
NASA GLENN
RESEARCH CENTER

2003
FINAL REPORT

NASA-OAI COLLABORATIVE AEROSPACE RESEARCH AND FELLOWSHIP PROGRAM

AT

NASA GLENN RESEARCH CENTER

AT LEWIS FIELD

CLEVELAND, OHIO

PREPARED BY THE CO-DIRECTORS:

ANN O. HEYWARD
VICE PRESIDENT, WORKFORCE ENHANCEMENT
OHIO AEROSPACE INSTITUTE

MARK D. KANKAM
UNIVERSITY AFFAIRS OFFICER
NASA GLENN RESEARCH CENTER

CONTENTS

INTRODUCTION

During the summer of 2003, a 10-week activity for university faculty entitled the NASA-OAI Collaborative Aerospace Research and Fellowship Program (CFP) was conducted at the NASA Glenn Research Center in collaboration with the Ohio Aerospace Institute (OAI). This is a companion program to the highly successful NASA Faculty Fellowship Program and its predecessor, the NASA-ASEE Summer Faculty Fellowship Program that operated for 38 years at Glenn. The objectives of CFP parallel those of its companion, viz.,

> (1) to further the professional knowledge of qualified engineering and science faculty,
> (2) to stimulate an exchange of ideas between teaching participants and employees of NASA,
> (3) to enrich and refresh the research and teaching activities of participants' institutions, and
> (4) to contribute to the research objectives of Glenn.

However, CFP, unlike the NASA program, permits faculty to be in residence for more than two summers and does not limit participation to United States citizens. Selected fellows spend 10 weeks at Glenn working on research problems in collaboration with NASA colleagues and participating in related activities of the NASA-ASEE program.

This year's program began officially on June 2, 2003 and continued through August 8, 2003. Several fellows had program dates that differed from the official dates because university schedules vary and because some of the summer research projects warranted a time extension beyond the 10 weeks for satisfactory completion of the work. The stipend paid to the fellows was $1200 per week and a relocation allowance of $1000 was paid to those living outside a 50-mile radius of the Center.

In post-program surveys from this and previous years, the faculty cited numerous instances where participation in the program has led to new courses, new research projects, new laboratory experiments, and grants from NASA to continue the work initiated during the summer. Many of the fellows mentioned amplifying material, both in undergraduate and graduate courses, on the basis of the summer's experience at Glenn. A number of 2003 fellows indicated that proposals to NASA will grow out of their summer research projects. In addition, some journal articles and NASA publications will result from this past summer's activities. Fellows from past summers continue to send reprints of articles that resulted from work initiated at Glenn.

This report is intended primarily to summarize the research activities comprising the 2003 CFP Program at Glenn.

RESEARCH SUMMARIES

Brief summaries of the fellows' research assignments follow. As is clear from the reports, some of the work is of sufficient importance and content to warrant reporting in the technical literature.

SPECIAL ACKNOWLEDGEMENT

The participants in the NASA-OAI Collaborative Aerospace Research and Fellowship Program sincerely express their recognition of service of Dr. Francis J. Montegani who retired as Chief, Office of University Programs at NASA Glenn Research Center. We wish him well in his future endeavors.

Name: **Aryeh A. Frimer**
Education: Ph.D., Chemistry
Harvard University

Permanent Position: Professor, Chemistry
Bar-Ilan University

Host Organization: Materials Division
Colleague: 5160/MaryAnn Meador

Assignment:

Design of New End Caps for More Thermal Oxidatively Stable Polymers

Norbornenyl end capped polyimides are widely used as polymer matrix composite materials for aircraft engine applications, since they combine ease of processing with good oxidative stability up to 300°C. PMR resins are prepared via a two-step approach involving the initial formation of oligomeric pre-polymers capped at both ends by a reactive end cap. The end cap undergoes crosslinking during processing, producing the desired low density, high specific strength materials. It is the end cap that facilitates processing by controlling molecular weight of the oligomer and allowing flow before crosslinking. However, it is this very end cap that accounts for much of the weight loss in the polymer on aging in air at elevated temperatures. Designing new end caps to slow down degradation has the potential to substantially prolong the lifetime of the material.

Previously, we reported studies on ^{13}C labeled PMR-15 in which we followed the thermo-oxidative aging of end cap by solid NMR. Based on the study, two major pathways of end cap degradation were identified. One path leads to much weight loss in the polymer. The other leads to more stable structures that form a protective layer on the surface. We are working toward the design of new end caps that favor the latter type of degradation. Several different structures are currently under investigation.
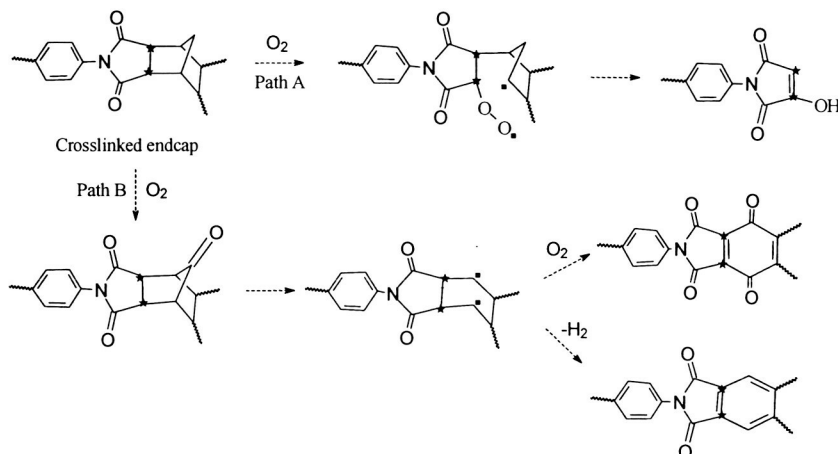
Research Summary Submitted by Fellow:

Reevaluation of Tetrahydrophthalic Anydrides as Endcaps for Improved Oxidation Resistance in Addition to Polyimides

A polyimide is a polymer composed of alternating units of diamine and dianhydride, linked to each other via an imide bond. PMR polyimides, commonly used in the aerospace industry, are generally capped at each end by an endcap (such as the nadic endcap used in PMR 15) which serves a double function: (1) it limits the number of repeating units and, hence, the average molecular weight of the various polymer chains (oligomers), thereby improving processability; (2) Upon further treatment (curing), the endcap crosslinks the various oligomer

3

strands into a tough heat-resistant piece. It is this very endcap, so important to processing, that accounts for much of the weight loss in the polymer on aging in air at elevated temperatures. Understanding this degradation provides clues for designing new endcaps to slow down degradation, and prolong the lifetime of the material.
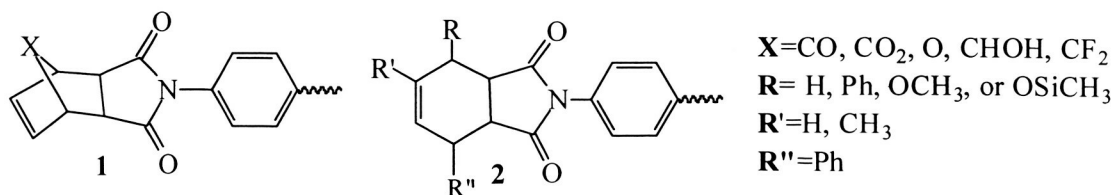
We have previously reported[1,2] studies on the thermo-oxidative aging of a modified PMR-15, in which we labeled the endcap at the methyne carbon □to the carbonyl groups with ^{13}C (shown in the Scheme 1 below labeled with a star).
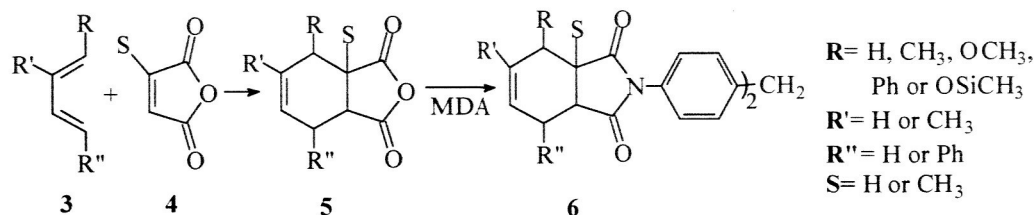
Scheme 1: PMR Degradation Pathways

Though aging is a complex process, by following the transformation of just this carbon by solid NMR, we have been able to identify two major degradation pathways for endcap oxidation. Path A produces cleavage products which lead to large weight losses, while path B forms stable oxidation products with much smaller associated weight losses. These stable products also help to form a surface layer on the polymer that protects the interior from further oxidation.

We have embarked on the synthesis of replacement endcaps that favor path B and lead to lower weight loss and, hence, less shrinkage and cracking in the oxidation layer.[3] We have proposed to utilize structures like **1** below. Our theory is that using an X group <u>more</u> labile than the methylene in the parent norbornenyl-end cap could actually <u>improve</u> oxidative stability. Recently, we reported on our exploration of the effect of replacing the nadic end-cap of PMR-15 with the 7-hydroxy analog of nadic anhydride (X=CH-OH).[4]

X=CO, CO$_2$, O, CHOH, CF$_2$
R= H, Ph, OCH$_3$, or OSiCH$_3$
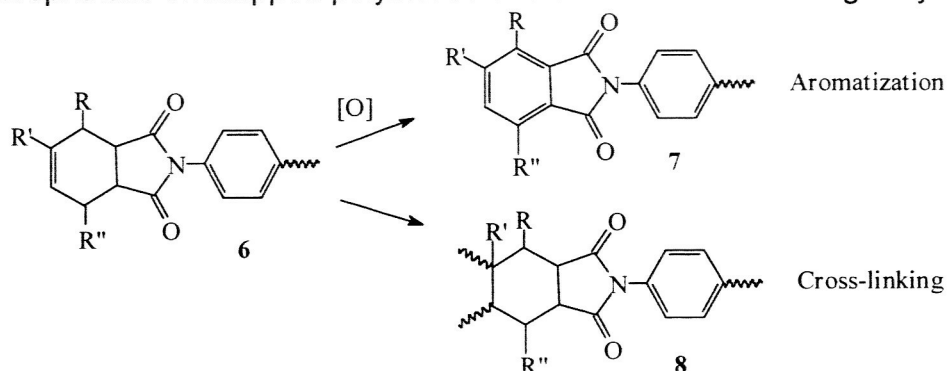**R'**=H, CH$_3$
R"=Ph

However, we must also consider 1,2,3,6-tetrahydrophthalimide **2** as an end cap that contains no X group at all. This structure was investigated by TRW and at NASA in the 1980's and found to yield composites with TOS values better than PMR-15, but quite frangible.[5] St. Clair and St. Clair[6] as an end cap for polyimide adhesives. However, they found no evidence of cross-linking in this system until 415°C. If the cross-linking temperature could be lowered—either by substitution on the ring or by catalysis—this might be a viable replacement for the norbornene end cap. Indeed, onset of decomposition for polymers made with this end cap was shown to be at a higher temperature than for the norbornenyl-end cap.

We have synthesized several substituted tetrahydrophthalic anhydride endcaps, including the 3-hydro, 3-phenyl, 3-methoxy, 3-trimethylsilyloxy, 4-methyl, 2,3-dimethyl and 3,6-diphenyl analogs via the Diels-Alder condensation of the corresponding butadienes and maleic or citraconic anhydride. The resulting anhydrides were then reacted with MDA generating imides **6**.

$R=$ H, CH_3, OCH_3, Ph or $OSiCH_3$
$R'=$ H or CH_3
$R''=$ H or Ph
$S=$ H or CH_3

These PMR model compounds (n=0) were heated gradually to 370 °C (700 °F) and the thermal-oxidative transformations followed by NMR. Analysis of the data indicates that when S=H, the tetrahydrophthalic endcaps undergo not only cross-linking, but aromatization as well. It is this substantial percentage of aromatic product that is responsible for both the observed improved TOS tetrahydrophthalic endcapped polyimides and their substantial frangibility.

When the thermolysis is carried out under inert atmosphere, aromatization was largely inhibited. When S=CH₃, aromatization was totally inhibited. We are currently investigating the thermal-oxidative stability of tetrahydrophthalic endcapped polyimides either processed under inert atmosphere or those in which aromatization is inhibited by the substitution pattern on the endcap.

Some of these results have been submitted for publication.[7]

References and Notes

[1]   Meador, M. A. B.; Johnston, J. C.; Cavano, P. J.; Frimer, A. A. *Macromolecules* **1997**, *30*, 3215-3223.

[2]   Meador, M. A. B.; Johnston, J. C.; Frimer, A. A.; Gilinsky-Sharon, P. *Macromolecules* **1999**, *32*, 5532-5538.

[3]   Meador, M. A. B.; Lowell, C. E.; Cavano, P. J.; Herrera-Fierro, P. *High Perform. Polym.* **1996**, *8*, 363-379.

[4]   (a) Meador, M. A. B.; Johnston, J. C.; Hardy-Green, D.; Frimer, A. A.; Gilinsky-Sharon, P.; Gottlieb, H.E. *Chemistry of Materials,* **13**, 2649-2655 (2001); (b) Meador, M. A. B.; Frimer, A. A. *NASA Tech Briefs*, October 2001, LEW-16987. This paper was awarded a NASA Certificate of Recognition for Technical Innovation. (c) Meador, M. A. B.; Frimer, A. A. U.S. Patent Number 6,303,744, October 16, 2001.

[5]   Alston, W.B. personal communication (August 2002) regarding unpublished results.

[6]   St. Clair, A. K.; St. Clair, T. L. *Polym. Eng. Sci.* **1982** *22*, 9-14.

[7]   Meador, M.A.B.; Frimer, A.A. *Polym. Prepr.,* **2003**, *44* (1), 240-241. M.A.B. Meador and A.A. Frimer, *NASA Tech Briefs*, 00, LEW-17429 (In press). Meador, M.A.B.; Frimer, A.A.; Johnston, J.C. (Submitted for Review).

Name: **Vladimir V. Golubev**
Education: Ph.D., Aerospace Engineering
University of Notre Dame

Permanent Position: Assistant Professor, Aerospace Engineering
Embry-Riddle Aeronautical University

Host Organization: Structures and Acoustics Division
Colleague: 5940/James R. Scott

Assignment:

Development of Implicit Time Marching for
Viscous Computational Aeroacoustics (CAA) Calculations

Implement highly stable, implicit time marching schemes in the Acoustics Branch CAA code for application to viscous CAA problems. Assess the relative benefits of low order versus high order schemes. Implement appropriate acceleration algorithms for sub-iteration convergence and evaluate performance. Conduct a study of viscous gust airfoil interaction for a thick, loaded Joukowski airfoil. Examine the effects of viscosity on the nonlinear airfoil response.

Research Summary Submitted by Fellow:

Further Development and Implementation of Implicit Time Marching in the
CAA Code

The fellowship research project continued last-year work on implementing implicit time marching concepts in the Broadband Aeroacoustic System Simulator (BASS) code. This code is being developed at NASA Glenn for analysis of unsteady flow and sources of noise in propulsion systems, including jet noise and fan noise.

The rationale for using an A-stable implicit time marching scheme, particularly for planned in the future Very Large Eddy Simulations (VLES) of unsteady fan stage and jet flows, is based on the following arguments. The choice between explicit and implicit marching schemes is governed by the ratio of the physical time scale (determined by the minimum required wave resolution), and the stability-dictated time scale. Explicit schemes are usually the best choice (in computational efficiency, overall accuracy and cost) when such scales are comparable, so that the resulting CFL numbers ~ 1. Implicit schemes are more efficient when the physical time scale is much larger compared to stability-dictated time scale, thus producing CFL ~ 10^3-10^4 in the regions of interest. For instance, both in time-accurate Euler simulations and DNS/LES of wall-bounded flows, CFL numbers determined by the required accuracy of both spatial and temporal resolutions, are small, and hence explicit schemes are typically employed. In steady-state Euler simulations, the time accuracy is not an issue, and the solution, obtained, e.g., by

pseudo-time marching, must be driven to the converged state as fast as possible (hence, the effective CFL $\rightarrow \infty$, and implicit time marching is preferred). Finally, in VLES or RANS of wall-bounded turbulent flows, CFL numbers in the near-wall regions can also be very high, of the order of 10^3-10^6. Indeed, in VLES simulations of jet noise, the effective CFL numbers are determined by the smallest grid size in the boundary layer of the nozzle, with the close to steady-state evolution of the latter producing the initial condition for the jet mixing layer at the nozzle lip. On the other hand, the grid size required to capture the large-scale coherent structures in the jet region and resolve acoustic propagation in the outside linear field is much larger, hence resulting in large CFL numbers. A similar situation is encountered in unsteady simulations of viscous flow around an airfoil, where the stability constraint is imposed by the boundary-layer resolution but the required time accuracy is governed by a much coarser mesh in the outer inviscid field. Thus, in both cases of jet and fan noise VLES, the implicit time marching capability is most essential for computationally efficient simulations.

The current, working version of the BASS code uses an explicit fourth-order Runge-Kutta scheme (RK56) for time stepping, to ensure accurate wave resolution through the smallest grid cells. While this is appropriate for inviscid flow grids where the range of grid cell sizes is small, it is not efficient for highly clustered viscous flow grids due to the excessively small time step required for stability. On the other hand, to become an effective tool, the iterative procedure implemented at each time step of the implicit time marching must converge quickly, with minimal numerical overhead. As part of the efforts during the last-summer program, a low-order implicit scheme was examined with simple corrector-type functional subiterations, computationally efficient for non-stiff

$$\frac{\Delta \vec{Q}^n}{\Delta t} = -\left(\frac{\beta}{1+\omega}\right) \vec{R}^{n+1} - \left(\frac{1-\beta}{1+\omega}\right) \vec{R}^n + \left(\frac{\omega}{1+\omega}\right) \frac{\Delta \vec{Q}^{n-1}}{\Delta t}$$

$$\Delta \vec{Q}^n = \vec{Q}^{n+1} - \vec{Q}^n$$

$$(E): \beta = 0, \quad (I): \beta \neq 0$$

problems. This summer work focused on investigating and implementing a low-order scheme with accelerated and robust convergence capability, thus applicable to more stiff problems. Both low-order implicit schemes are derived from a basic nonlinear scheme, which is up to second-order accurate and may lead to implicit *(I)* or explicit *(E)* formulation depending on the choice of parameter β. In application to governing nonlinear equations written in the form where the time variation of solution is the only term on the left-hand side (LHS), the basic nonlinear scheme is,

(1)

The selected first-order backward Euler algorithm reduces (1) to

$$\frac{\Delta \vec{Q}^{n,l+1}}{\Delta t} = -\vec{R}^{n+1,l+1}, \quad l = 1, 2, \dots$$

which, following RHS linearization, results (for 2D case) in

$$(\frac{\vec{I}}{\Delta t} + \vec{J}^n)\Delta\vec{Q}^n = -\vec{R}^n, \quad \vec{J}^n = \frac{\partial\vec{R}^n}{\partial\vec{Q}} = \frac{\partial\vec{F}_x^{\,n}}{\partial\vec{Q}} + \frac{\partial\vec{F}_y^{\,n}}{\partial\vec{Q}} = \vec{A} + \vec{B}$$

(2)

In the method with functional subiterations, the Jacobian matrix is omitted, thus resulting in the following previously implemented scheme (IMPC) with dual time stepping (with indices n and l denoting the physical time and the pseudo-time

$$\Delta\vec{Q}_{RES}^{n,l} = \vec{Q}^{n+1,l+1} - \vec{Q}^{n+1,l} \to 0, \quad l \to \infty$$

$$\frac{\Delta\vec{Q}_{RES}^{n,l}}{\Delta\tau} = -\frac{\vec{Q}^{n+1,l} - \vec{Q}^n}{\Delta t} - \vec{R}^{n+1,l} = -(\vec{R}^*)^{n+1,l}$$

steps, respectively):

Note that the pseudo-time parameter τ governs the subiteration process, and does not affect the actual time accuracy of the scheme which remains first-order accurate. The new implemented scheme preserves the dual time stepping, but in addition employs the Jacobian matrix to accelerate convergence and make subiterative process more reliable both for stiff and non-stiff problems. The

$$[\frac{\vec{I}}{\Delta\tau} + (A_{ij}^+ + B_{ij}^+ - A_{ij}^- - B_{ij}^-)]\Delta\vec{Q}_{ij}^* = \{-A_{i+1,j}^-\Delta\vec{Q}_{i+1,j}^* - B_{i,j+1}^-\Delta\vec{Q}_{i,j+1}^*\} - \vec{R}_{ij}^{*(n+1,l)},$$

$$\vec{R}_{ij}^{*(n+1,l)} = \left\{\frac{\vec{Q}_{ij}^{n+1,l} - \vec{Q}_{ij}^n}{\Delta t}\right\} - \vec{R}_{ij}^{n+1,l}$$

particular idea of treating LHS of (2) is based on Jameson and Yoon's implementation of positive/negative Steger-Warming flux-splitting of Jacobians in (2), leading to the LU-SSOR method. The resulting scheme is implemented in two (backward and forward) sweeps of the computational domain:

(3a)

$$[\frac{\vec{I}}{\Delta\tau} + (A_{ij}^+ + B_{ij}^+ - A_{ij}^- - B_{ij}^-)]\Delta\vec{Q}_{RES(ij)}^{n,l} = \{A_{i-1,j}^+\Delta\vec{Q}_{RES(i-1,j)}^{n,l} + B_{i,j-1}^+\Delta\vec{Q}_{RES(i,j-1)}^{n,l}\} +$$

$$\left\{\frac{\vec{I}}{\Delta\tau} + (A_{ij}^+ + B_{ij}^+ - A_{ij}^- - B_{ij}^-)\right\}\Delta\vec{Q}_{ij}^*,$$

$$\Delta\vec{Q}_{RES}^{n,l} = \vec{Q}^{n+1,l+1} - \vec{Q}^{n+1,l} \to 0, \quad l \to \infty$$

(3b)

The results of numerical tests were examined for the case of a Gaussian low-amplitude density pulse in a 2D domain with Cartesian grid and periodic boundary conditions. The calculated contour plots for the density pulse are shown after marching in time for 0.2 sec following introduction of the pulse at the center of the domain. Figures 1 and 2 compare results from the two implicit

schemes with functional correction (IMPC) and LU-SSOR algorithm (LUSR). As expected, different LHS treatments kept the overall accuracy of the scheme determined by RHS in (2), and thus produced identical results. However, LUSR converged to the imposed residual tolerance of 10^{-9} with less number of subiterations per time step (e.g., for CFL=1.25, it took LUSR 27 subiterations vs. 32 for IMPC, for the first time step). Convergence of both schemes is affected both by CFL number and the relaxation factor $\Delta\tau/\Delta t$. In LUSR, an additional parameter is introduced affecting the spectral radii of the modified Jacobian matrices $A^{\pm}$ and $B^{\pm}$. in (3), and thus the convergence rate. Future work will examine further optimization of the algorithm for faster convergence rates. Note that compared to the time-accurate solution using RK56 in Figure 3, the implemented backward Euler schemes are highly dissipative and (moderately) dispersive. The time-accurate solution for LUSR is recovered in Figure 4 when using a small time step (CFL=0.1). On the other hand, as mentioned before, for many problems of interest, a low-order implicit scheme may be adequate since the accuracy of time marching is critical only in the outer region, where adequate time steps mean very large CFL numbers in the near-wall viscous layers. Thus, the strategy is to select CFL numbers as required for time-accurate unsteady flow resolution in the outer region, while ensuring stability of time marching in the near-wall viscous region. The ability of the LUSR scheme to maintain stable time marching in such zones with higher CFL numbers is illustrated in Figure 5. The plans for the future work include testing the strategy for the time-implicit simulation of unsteady viscous flow around an airfoil.

The progress on the Fellowship research was reported at the presentation "Progress in Implementation of Implicit Time Marching in the Broadband Aeroacoustic System Simulator (BASS) Code" given for the Structures and Acoustics Division on June 11, 2003.
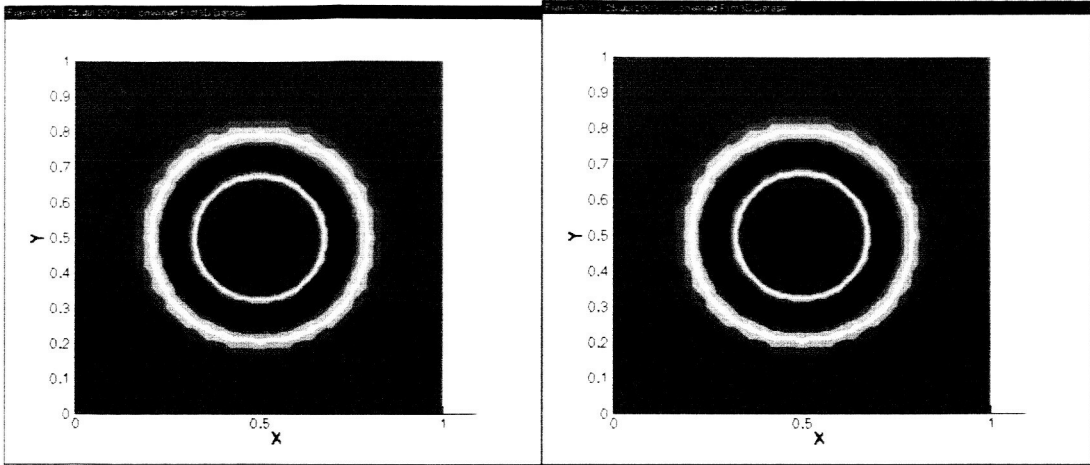
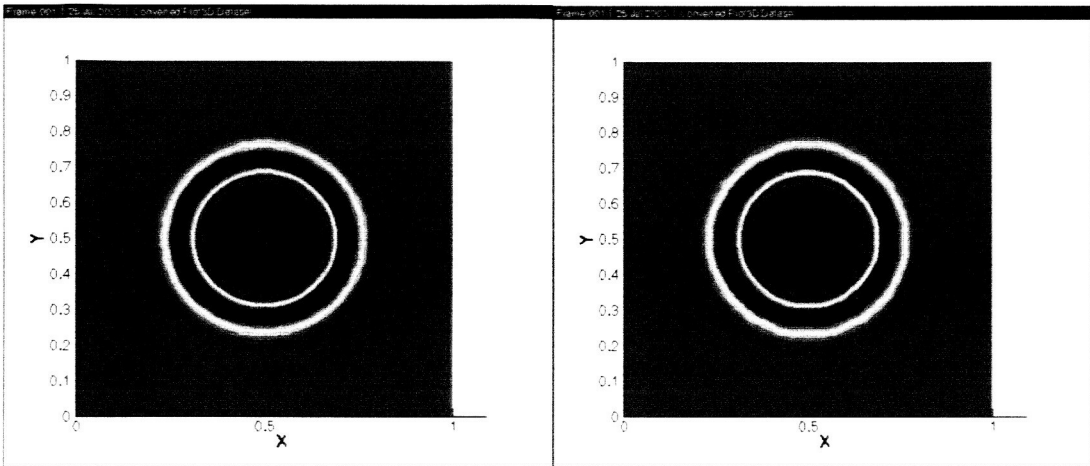Figure 1: LUSR, CFL=1

Figure 2: IMPC, CFL=1

Figure 3: RK56, CFL=1
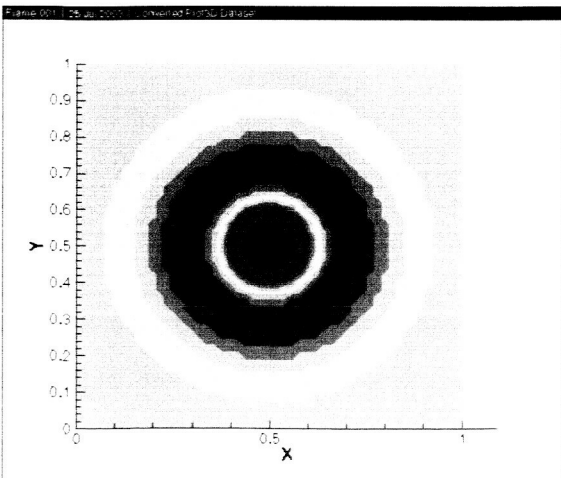

Figure 4: LUSR, CFL=0.1

Figure 5: LUSR, CFL=4

11

Name:	**Ming-Chia D. Lai**
Education:	Ph.D., Mechanical Engineering
	Pennsylvania State University

Permanent Position:	Professor, Mechanical Engineering
	Wayne State University

Host Organization:	Turbomachinery and Propulsion Systems Division
Colleague:	5830/Robert R. Tacina

Assignment:

The fellowship work this summer will be in support of the development of a fuel mixer for a liquid fuel reformer that is upstream of a fuel cell. Tasks for the summer shall consist of design of a fuel mixer, setup of the laser diagnostics for determining the degree of fuel mixing, and testing of the fuel mixer. The fuel mixer shall be a venturi section with fuel injected at or near the throat, and an air swirler upstream of the venturi. Data to determine the performance of the mixer shall be taken using a Phase Doppler Particle Analyzer (PDPA).

Research Summary Submitted by Fellow:

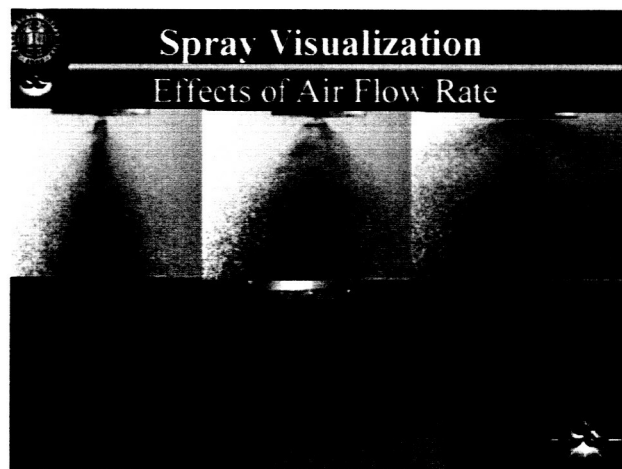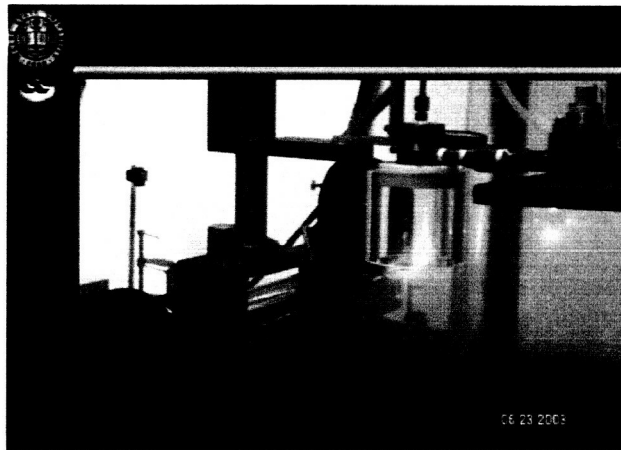## Fuel Reformer Nozzle Development

Activities:

- Set up spray visualization and phase-Doppler interferometry instrumentation.
- Carry out characterization of SVT nozzle spray.
- Setup grid generation and CFD computation of swirler-venturi flow field (ref:1,2)
- Compare different nozzle design and evaluate performance requirement for fuel reformer application.
- Review and seminar presentation of automotive injector technologies
- Written report and seminar presentation of SVT nozzle characterization
- Semianr presentation and power point report of CFD results of swirler-venturi nozzle
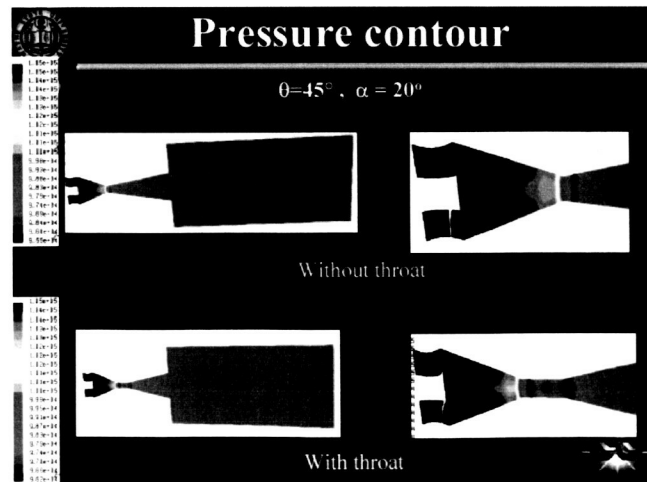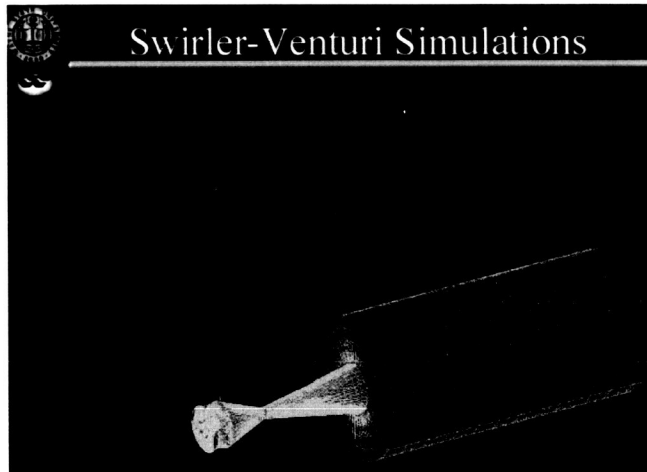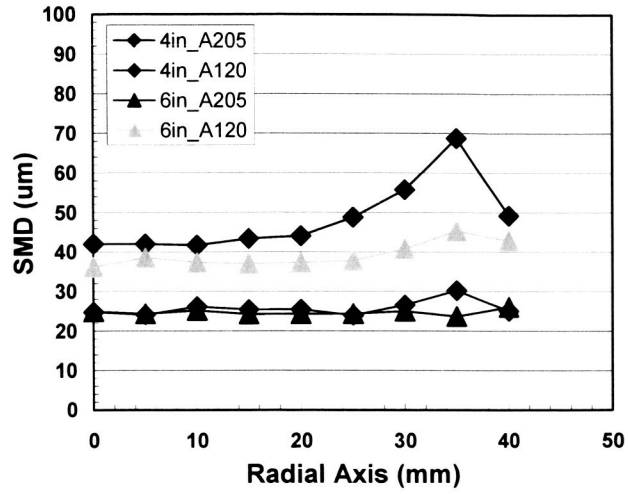- Prepare abstract for AIAA Aerospace Science Meeting, Reno, and January, 2004.

Reference:

[1] Sun, H., Chue, T. H., Lai, M.-C., and Tacina, R. (1997) "Atomization Characteristics of Capillary Fuel Injection inside a Venturi Nozzle," *Atomization and Sprays,* Vol. 7, pp. 245-265.
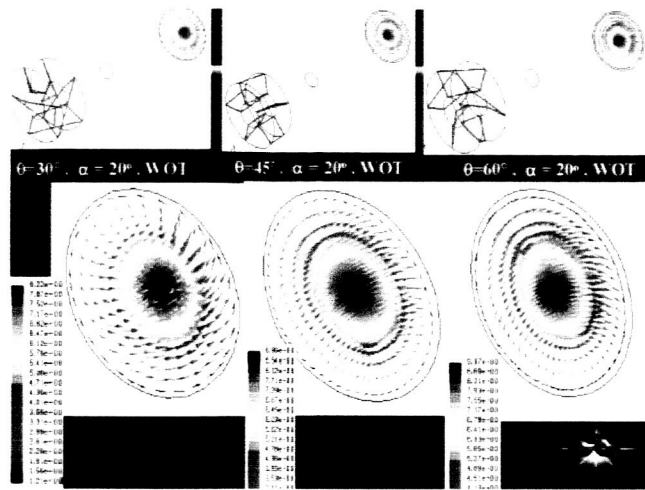
[2]   Im, K., Lai, M.-C., and Tacina, R. (2001) "Parametric Studies of Swirl Venturi Tube Injectors," AIAA *J. Propulsion and Power*, 17(3), pp.717-727.

[3]   Lai, M.-C., Im, K.-S., and Tacina, R. (2004) ""Spray and Fuel-Air Mixing of the Swirler/Venturi Injectors for Fuel Reformer" abstract accepted by AIAA Aerospace Science Meeting, Reno, January, 2004.

Major results:

Mean Diameter
Sauter Mean Diameter

Swirler-Venturi Simulations

Pressure contour

$\theta = 45°$, $\alpha = 20°$

Without throat

With throat

θ=30°, α = 20°, WOT   θ=45°, α = 20°, WOT   θ=60°, α = 20°, WOT

Name:	**Ivana M. Milanovic**
Education:	Ph.D., Mechanical Engineering
	Polytechnic University

Permanent Position:	Assistant Professor, Mechanical Engineering
	University of Hartford

Host Organization:	Turbomachinery and Propulsion Systems Division
Colleague:	5860/Khairul B. Zaman

Assignment:

During the past two summers Professor Milanovic conducted Wind tunnel experiments on steady jets-in-cross-flow and synthetic jets. In her anticipated visit during the upcoming summer, she will continue and complete the research on synthetic jets involving 2-dimensional orifices of different aspect ratio as well as inclined slots. In addition, experiments will be conducted on pulsatile jets-in-cross-flow. The pulsation will be provided via an oscillating valve at controllable frequencies. The experiment will involve mainly hot-wire anemometer measurements in the low-speed wind tunnel. Overall goal will be to obtain database and investigate flow control strategies. The research will be of fundamental nature. The wind tunnel facilities are located in the Test Cells CW13 and CW15 of the Engine Research Building. I, as NASA colleague, will be directly collaborating with her in these experiments. Dr. Gerard Welch of the Compressor Branch (5810) will also be involved in this research effort.

Research Summary Submitted by Fellow:

An Experimental Study of Synthetic Jets from Rectangular Orifices

An experimental investigation on synthetic jets from rectangular orifices with and without cross-flow has been conducted in the NASA GRC subsonic wind tunnel. Additionally, a comparative study of synthetic jets from round orifices and their steady counterparts was carried out. In recent research synthetic jets have emerged as a promising active flow control tool since they introduce flow perturbation without a net mass injection. Thus, there is no requirement for bleed fluid and minimal demand for additional hardware. Potential benefits include alleviation of separation in inlets and ducts, stall margin improvement for turbomachinery, mixing enhancement in jet exhausts and combustors, lift augmentation and drag reduction for wings as well as noise suppression.

A synthetic jet is created from the ambient fluid by impressing an oscillating pressure gradient across an orifice. Suction pressure entrains the fluid into the orifice, and during the discharge phase flow separates at the edges forming a shear layer. The vortex sheet then rolls up and advects away under its own

16

induced velocity. Consequently, a net momentum is transferred to the surrounding fluid even though the net mass flux is zero.

In terms of basic research, while extensive work has been done on the structure and dynamics of an isolated synthetic jet, its behavior in a cross-flow (SJCF) has been addressed in relatively few investigations. For a given synthetic jet, the effect of varying cross-flow velocity (i.e., 'momentum-flux ratio') has not been studied systematically. Also, in applications the orifice geometry could often be complex involving pitch and yaw. Detailed flow-field information including vorticity and turbulent stresses, useful for simulation and development of models, are also lacking. Finally, most previous works involved relatively low Reynolds number jets, and an exploration at higher Re was deemed appropriate. These provided the motivation for a further investigation.

The experiments were conducted in a NASA GRC low speed wind tunnel with 30 x 20 in test section shown in Fig. 1. Synthetic jets were created by a loudspeaker (Altec Lansing 16 in. woofer) housed in a chamber underneath the test section as seen in Fig. 2. Rectangular and round orifices were straight holes cut through a thick clear plastic plate, 10 in. diameter by 0.5 in. and 1 in., respectively. Discs were mounted flush on the test section floor. Rectangular geometries were of aspect ratio 4:1, 8:1 and 16:1. Orifice pitch, measured between the nozzle centerline and the floor of the test section was $\alpha = 90°$. Additional configuration with 8:1 aspect ratio was set at $\alpha = 20°$. Disk could be rotated to vary the yaw angle, β, measured between the nozzle centerline and the direction of the cross-flow. Round jets were of the orifice diameter, $D = 0.75$ in. The equivalent diameter based on the area of cross-section through which the flow perturbation discharged into the cross-flow was the same for all cases, $D = 0.75$ in.

In order to obtain highest sound pressure amplitudes Helmholtz resonance of the chamber was utilized. However, off-resonance frequencies were employed when requiring smaller amplitudes. Sinusoidal functions were used to drive the woofer. For a given frequency, the amplitude of the pulsatile flow was controlled by varying the input voltage, A, to the woofer.

The measurements were performed by standard hot-wire anemometry. Two x-wires, one in 'u-v' and the other in 'u-w' configuration, were used for flow mapping in the cross-flow plane. The probes were stepped through the same grid points allowing the measurement of all three components of mean velocity and turbulence intensity. A single element of the 'u-w' wire, with appropriate calibration, was used to measure the velocity characteristics at the exit of the orifice. The origin of the coordinate system is located at the center of the orifice as illustrated in Fig. 2. The streamwise or cross-stream direction (parallel to the tunnel flow) is denoted by x, the direction normal to the tunnel floor is denoted by y, and the spanwise direction along the tunnel floor by z. The approach boundary layer was turbulent with a thickness about 60% of the orifice diameter.

The characteristic velocity and length are the average velocity ($\bar{V}$) and the equivalent length (L_0) of a slug of fluid expelled during the discharge half of the cycle, respectively. In order to evaluate $\bar{V}$ and L_0 the hot-wire time traces were phase-averaged using the signal to the loudspeaker as reference. The peak amplitude of the trace during the discharge together with the trough in the middle are utilized to estimate $\bar{V}$ and L_0, assuming a sinusoidal function. The parameters for representative rectangular cases of the study are listed in Table 1.

Distributions of phase-averaged properties were obtained with the same x-wire survey scheme, using the input to the woofer as a reference. Data were acquired for 19 phases within the period of perturbation. Selected phase-averaged velocity contours at $z/D = 0$ are shown for the 8:1 orifice in Fig. 3. These data capture the unsteady cycling of the synthetic jet in the cross-flow and provide a clear perspective of the events leading to the time-averaged field seen in Fig. 4. Figure 4 shows streamwise vorticity distribution for 8:1 orifice with 90° yaw (major axis of orifice perpendicular to the cross-flow) and 5 equivalent diameters downstream the exit. The frequency is 33 Hz and the tunnel velocity is 23 ft/sec. The amplitude corresponds to a momentum-flux ratio of about 6. A pair of counter-rotating vortices, similar to the 'bound vortex pair' of a steady JICF, is observed.

Comparison of flow-fields between SJCF and JICF was done for the case of normal injection from round orifice and a range of momentum-flux ratios ($J \le 16$). Distributions of mean velocity, streamwise vorticity and turbulence intensity are found to be similar. In Figs. 5 and 6 the mean velocity distributions are shown for $J = 12$, comparing SJCF with JICF. Mean velocity field exhibits a 'dome' of low momentum fluid pulled up from the boundary layer and the entire domain is characterized by high turbulence. When the maximum velocity during the discharge stroke of a SJCF equals the exit velocity of a JICF, the penetration of the two are found to be comparable for a given cross-flow. For the JICF with increasing J, a change in the flow-field topology has been noted. Below $J \approx 3$, only a velocity deficit is observed. At higher J, the 'dome' of low momentum fluid is capped by a kidney-shaped region of high momentum fluid as seen in Fig. 6. For SJCF with increasing J while the penetrations are similar the high momentum region is absent even at $J = 12$. A pair of counter-rotating streamwise vortices, corresponding to the 'bound vortex pair' of the steady case, is clearly observed. However, several differences are also noted. The magnitude of the velocity deficit, the strength of the streamwise vortex pair as well as the turbulence intensity is higher in the JICF case. For the SJCF there is a conspicuous vortex pair of opposite sense near the wall underneath the bound vortex pair. Only a hint of this can be seen with the JICF.

This comprehensive study will provide much needed experimental information related to the various control strategies. The results will be analyzed and documented in detail. Presentations at national conferences and publication of

peer-reviewed journal articles are also expected. Projected publications will present both the mean and turbulent properties of the flow field, comparisons made with the data available in an open literature where possible, as well as recommendations for the future work.

Case	Ratio	f (Hz)	A (Vrms)	V_{max}(ft/s)	$\overline{V}$	L_0/D	Re
1	4:01	33	0.5	4.4	2.8	1.4	2335
2	4:01	33	9.6	53.7	34.2	16.6	28503
3	8:01	33	0.22	1.7	1.1	0.5	902
4	8:01	33	0.6	5.7	3.6	1.8	3025
5	8:01	33	1.2	13.4	8.5	4.1	7113
6	8:01	33	2.2	22.3	14.2	6.9	11837
7	8:01	33	4.5	36.0	22.9	11.1	19108
8	8:01	33	9.6	53.0	33.8	16.4	28132
9	8:01	33	15	63.6	40.5	19.6	33758
10	16:01	33	0.35	3.5	2.2	1.1	1858
11	16:01	33	9.6	50.2	32.0	15.5	26645

Table 1 Initial condition for different SJ Configurations.
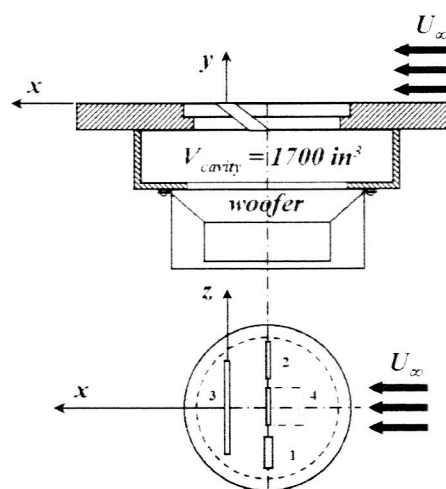

Fig. 1 Experimental Facility.

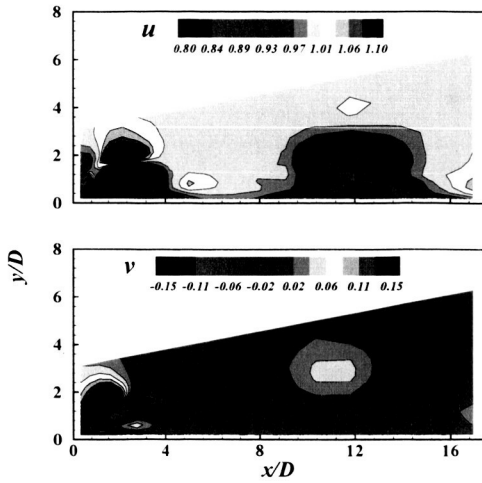Fig. 2 Experimental set up and rectangular orifice geometries: (1) 4:1, (2) 8:1, (3) 16:1, (4) 8:1, $\alpha = 20°$.

Fig. 3 Phase-averaged velocity contours for SJCF from rectangular orifice (8:1), $\alpha = 90°$, $\beta = 90°$.
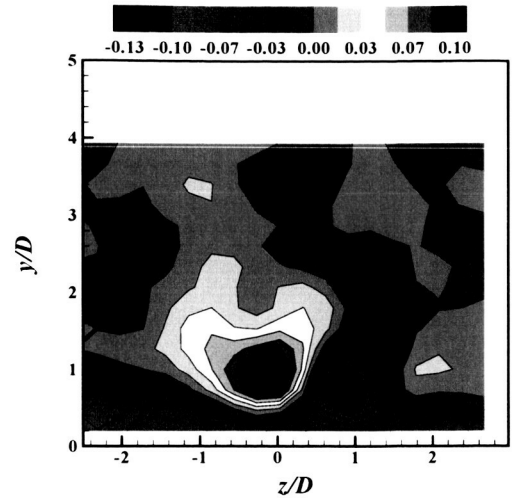

Fig. 4 Streamwise mean vorticity contours for SJCF from rectangular orifice (8:1), $\alpha = 90°$, $\beta = 90°$.
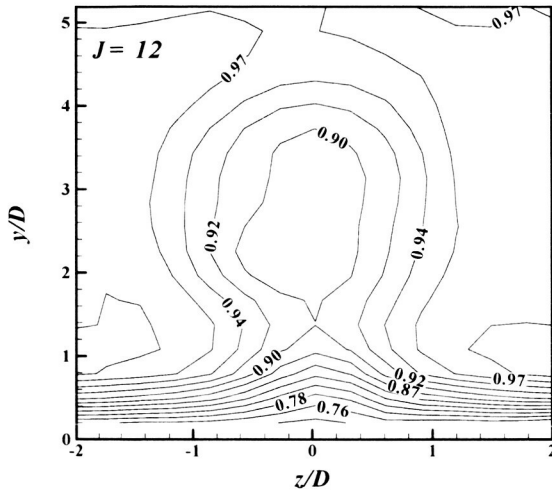

Fig. 5 Streamwise mean velocity contours for SJCF from cylindrical orifice; $x/D = 5$.
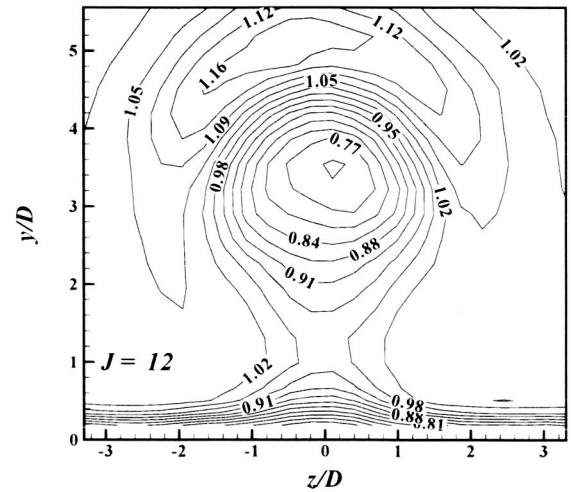

Fig. 6 Streamwise mean vorticity contours for JICF from cylindrical orifice; $x/D = 5$.

Name: **Jerzy T. Sawicki**
Education: Ph.D., Mechanical and Aerospace Engineering
Case Western Reserve University

Permanent Position: Professor, Mechanical Engineering
Cleveland State University

Host Organization: Structures and Acoustics Division
Colleague: 5920/George Y. Baaklini

Assignment:

Multi-Discipline Analytical Modeling of a Cracked Disk in a Turbine Engine: Applied to TF41 Experiment at China Lake

TASK I. Multi-discipline analytical modeling of the TF41 engine to assist in the analysis of vibration data collected during fan disk crack growth study at China Lake. Task should include:
- Determine critical speeds of the TF41 engine by full system rotordynamic analysis
- Determine of the changing system unbalance due to propagating crack in the fan disk
- Coordinate rotordynamics model, FE analysis of fan disk, and fracture mechanics model
- Compare and analyze the numerical prediction and the measured vibrations

TASK II. Develop fundamental understanding of the Pax River spin pit hanging shaft system
- Develop rotordynamics model of spin pit system
- Define speed-dependent eccentricity based on FE model of cracked disk
- Vibration data, FE source code and crack information will be provided by Hood Technologies

Research Summary Submitted by Fellow:

Multi-Discipline Analytical Modeling of a Cracked Disk in a Turbine Engine: Applied to TF41 Experiment at China Lake

The investigated crack detection method is based on the fact that the development of a disk crack results in a distorted strain field within the component. As a result, a minute deformation in the disk's geometry as well as a change in the system's center of mass occurs. Finite element analyses were conducted concerning a notched disk in order to define the sensitivity of the method. The notch was used to simulate an actual crack and will be the method utilized for upcoming experiments. Various notch sizes were studied and the geometric deformations and shifts of center of mass were documented as a

function of rotational speed. In addition, a rotordynamic analysis of a two-bearing, disk and shaft system was conducted. The results of the FE analyses of the disk indicated that the overall changes in the disk's geometry and center of mass were rather small. Comparing the 9.25 in. disk's maximum radial displacements due centrifugal forces at 8000 RPM between an un-notched and a 0.962 in. notched disk, the difference was on the order of 0.00014 in. The shift in center of mass was also of this magnitude. The next step involves running experiments to verify the analysis.

Figure 1 shows the final design of the subscale disk used for this study. The material of the disk is Haynes X-750 having density $\rho = 0.3 \, \text{lb/in}^3$, modulus of elasticity $E = 31 \, \text{Mpsi}$, Poisson's ratio $v = 0.31$, shear modulus $G = 11.83 \, \text{Mpsi}$, the ultimate tensile strength $S_{ut} = 145 \, \text{ksi}$, and yield strength $S_y = 95 \, \text{ksi}$. The damage representing a crack was introduced in the form of a circumferential notch located in the disk's web region (see Fig. 1). The notch width of 0.15 in. was based on the wire thickness and burn area of the electrical discharge machining (EDM) wire. Different lengths of notch were considered.
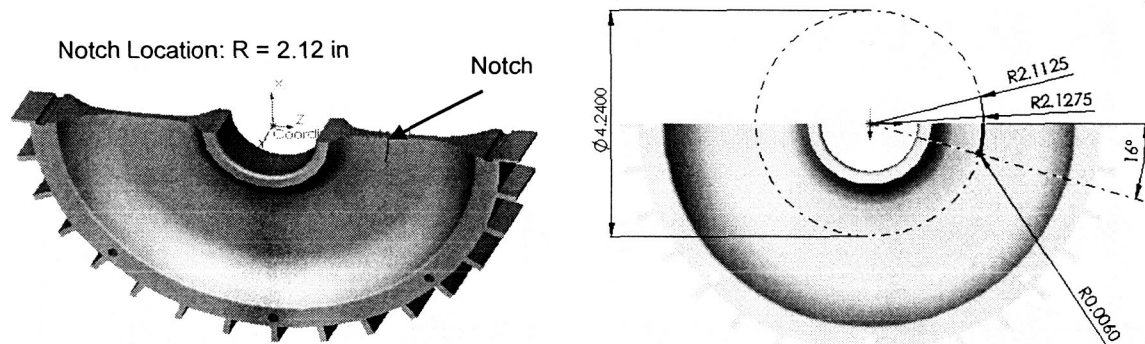

Figure 1 Notch dimensions for the particular case of a 1.184 in. notch length.

Figure 2 shows the stress state at the notch tip as a function of notch length and revolutions per minute (RPM). The results of the figure will be utilized in defining the experimental notch length and disk speed so as to maintain a safe test environment.
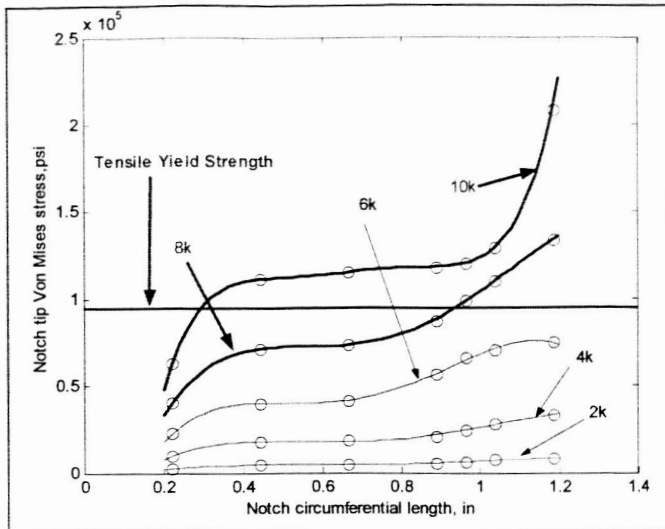
Figure 2. von Mises stress stresses at notch tip as a function of notch length and disk RPM.
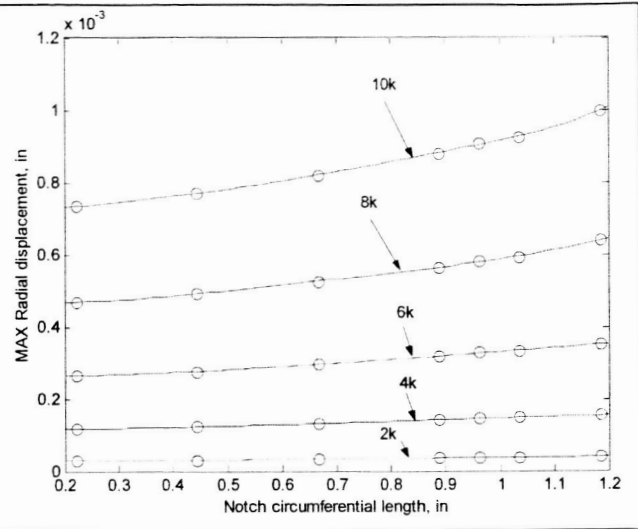
Figure 3. Maximum radial displacements as a function of notch length and disk RPM.

Figure 3 displays the maximum radial displacement due to centrifugal expansion as a function of notch length and rotational speed, while Fig. 4 displays the net change after subtracting the displacement values of an undamaged disk. Viewing figures 3 and 4, it is apparent that the notch-induced changes in the maximum displacement are rather small. For example, the net change in the maximum radial displacement of a notched disk (notch length = 0.962 in.) at 8000 RPM is 0.00014 in. This particular set of parameters is of interest due to the fact that it is experimentally feasible to test these conditions since the notch tip stress is below the yield strength of the material (see Fig. 2).
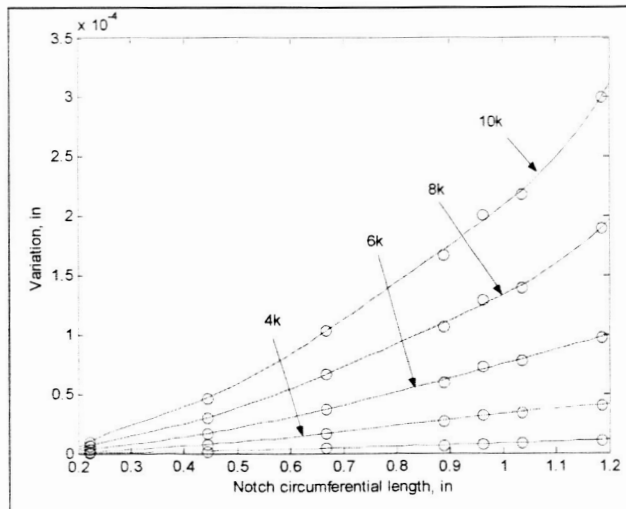

Figure 4. Net radial displacements after subtracting displacement values from an undamaged disk.
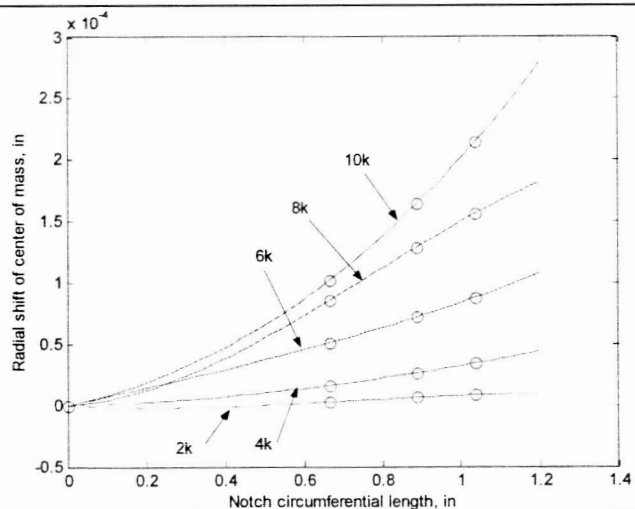
Figure 5. Radial shift of the center of mass as a function of notch length and disk RPM.

Figure 5 shows the approximate shift in the center of mass as a function of notch length and rotational speed. The values are similar in scale to the net change in radial displacement (see Fig. 4). Therefore, the global influence of the notch is revealed both in the deformation of the disk, as indicated by the change in the disk's maximum radial displacement, and in the isolated disk's center of mass shift.

Name: **Ana V. Stankovic**
Education: Ph.D., Electrical Engineering
University of Wisconsin, Madison

Permanent Position: Assistant Professor, Electrical and Computer Engineering
Cleveland State University

Host Organization: Power and On-Board Propulsion Technology Division
Colleague: 5450/Barbara Kenny

Assignment:

Professor Stankovic will be working to support the development of a power conditioning system to convert the 3 phase, 600 volt output of a permanent magnet generator to regulated DC power for ion thrust propulsion for a future spacecraft mission. Her work will involve developing a Simulink simulation of the generator with one of two alternative conversion schemes—a diode bridge with a chopper or a PWM regulated inverter. Ideally she will have enough time this summer to develop both simulations and compare them in terms of performance and anticipated losses and make a recommendation as to which is best suited for this application.

If there is additional time, the next step in the simulation process is to develop an "end-to-end" simulation that includes the generator, the preferred converter(s), and multiple ion thruster loads. (It is anticipated that each ion thruster load will have its own converter.)

At the end of her summer tenure, she will document her work in a written report and also as a 30-60 minute presentation to the Branch.

Research Summary Submitted by Fellow:

An Analytical Study of Diode Bridge Versus
PWM Rectifier for AC Spacecraft Power Systems

Although dynamic AC power generation systems have been designed in the past, all current spacecraft power systems have been DC systems, using DC power generation, storage, and distribution. A recent NASA study for a deep space missions has revived interest in dynamic systems using AC power generation. One of the areas of study in developing an AC system is AC to DC power conversion technology. The distribution system is required to supply power to several large independent DC loads. Some of these loads may be powered by the voltage obtained by "rectifying" the alternator output, others may require a higher or lower voltage, potentially obtained by a set-up or step-down transformer and "rectifier" arrangement. The primary objective of this study was to evaluate the relative merits of using an active Pulse width modulated (PWM) converter to rectify and regulate the DC output as compared to using a 3-phase

full wave diode bridge rectifier. A second part of the study was to investigate operating multiple PWM converters in parallel on the alternator bus. Two SIMULINK models have been developed and used to compare two different topologies for AC Spacecraft Power Systems.